Biochemical Journal (2021) **478** 2371–2384
https://doi.org/10.1042/BCJ20210267

PORTLAND PRESS

Research Article

Structure of plant photosystem I-plastocyanin complex reveals strong hydrophobic interactions

Ido Caspy[1,*], Mariia Fadeeva[1,*], Sebastian Kuhlgert[2,*], Anna Borovikova-Sheinker[1], Daniel Klaiman[1], Gal Masrati[1], Friedel Drepper[3], Nir Ben-Tal[1], Michael Hippler[2,4] and Nathan Nelson[1]

[1]Department of Biochemistry and Molecular Biology, The George S. Wise Faculty of Life Sciences, Tel Aviv University, Tel Aviv 69978, Israel; [2]Institute of Plant Biology and Biotechnology, University of Münster, 48143 Münster, Germany; [3]Institut für Biologie II, Universität Freiburg, Schänzlestr. 1, 79104 Freiburg, Germany; [4]Institute of Plant Science and Resources, Okayama University, Kurashiki, Japan

Correspondence: Michael Hippler(mhippler@uni-muenster.de) or Nathan Nelson (nelson@tauex.tau.ac.il)

Photosystem I is defined as plastocyanin-ferredoxin oxidoreductase. Taking advantage of genetic engineering, kinetic analyses and cryo-EM, our data provide novel mechanistic insights into binding and electron transfer between PSI and Pc. Structural data at 2.74 Å resolution reveals strong hydrophobic interactions in the plant PSI–Pc ternary complex, leading to exclusion of water molecules from PsaA–PsaB/Pc interface once the PSI–Pc complex forms. Upon oxidation of Pc, a slight tilt of bound oxidized Pc allows water molecules to accommodate the space between Pc and PSI to drive Pc dissociation. Such a scenario is consistent with the six times larger dissociation constant of oxidized as compared with reduced Pc and mechanistically explains how this molecular machine optimized electron transfer for fast turnover.

Introduction

Biological energy conversion relies on a sequence of redox reactions within the membrane-embedded electron transport chains of chloroplasts and mitochondria. In plants, the photosynthetic electron transport between the two photosystems has to cover distances of a few hundred nanometers. This is due to the unique architectural features of the photosynthetic thylakoid membranes, which fold into stacked grana and unstacked stroma thylakoids [1]. However, the thylakoid architecture and the configuration of the protein complexes are subject to constant modulation in response to environmental and physiological stresses [2–4]. Plastoquinone and plastocyanin (Pc) shuttles electrons from PSII to PSI, one within the hydrophobic milieu of the membrane and the second in the hydrophilic environment of the lumen [5]. Pc exploits specific binding sites on its electron donor — cytochrome f — and its electron acceptor — PSI [6]. The former interaction is a crude protein–protein interaction [7], and the latter is quite involved due to the onset of P700 oxidation at the ns time scale and the electron transfer from Pc that take place at the μs time scale [8–11].

Binding and electron transfer between Pc and PSI is driven by hydrophobic and electrostatic interactions [12]. In plants and green algae, the electron transfer reaction between Pc and PSI exhibits two distinct kinetic phases. A first fast microsecond intra-molecular electron transfer can be explained by a stable complex between PSI and Pc already formed prior to a flash. In the second slower phase, the remaining PSI complexes are re-reduced by the soluble donor in a bimolecular reaction with second-order kinetics. The occurrence of a preformed complex is dependent on the presence of the eukaryotic positively charged domain of subunit PsaF. The dissociation constant of oxidized Pc is about six times larger than that observed for reduced Pc [13], resulting in a 50–60 mV higher midpoint redox potential of Pc bound to PSI as compared with soluble Pc. This translates into a decrease in the driving force within the intra-molecular electron transfer complex, which is consistent with the fact that the P700 population is not fully reduced *in vivo* [14]. Moreover, single turnover flashes of isolated PSI fail to oxidize the whole P700 population [15,16].

*Equally contributed to the experimental work presented.

Received: 19 April 2021
Revised: 28 May 2021
Accepted: 3 June 2021

Accepted Manuscript online: 4 June 2021
Version of Record published: 23 June 2021

Biochemical Journal (2021) 478 2371–2384
https://doi.org/10.1042/BCJ20210267

In this work, we used the single particle cryo-EM technique to obtain a high-resolution structure of reduced Pc in complex with plant PSI and analyzed the interaction between the two complexes. For kinetic studies, a highly purified pea PSI derived from PSI crystals and purified pea Pc were employed.

Materials and methods

Pea $P700^+$ reduction

In all the kinetics measurements described in this work about 50 large pea PSI crystals were collected using 0.7–1.0 mm Cryoloop (Hampton research) and released into a 0.5 ml Eppendorf tube containing 0.4 ml solution of 50 mM K_2PO_4, 50 mM Tris (pH 8) and 20% PEG 400. Following centrifugation at 14 000 rpm for 1 min, the supernatant was carefully removed, and the crystals were solubilized in 60 µl of a solution containing 20 mM Tricine-Tris (pH 8) and 0.05% n-dodecyl-α-maltoside (αDM) at a chlorophyll concentration of 1–3 mg/ml.

Cryo-EM data collection and processing

For cryo-EM structural determination, about 50 large pea PSI crystals were collected using 0.7–1.0 mm Cryoloop (Hampton research) and released into a 0.5 ml Eppendorf tube containing 0.4 ml solution of 50 mM K_2PO_4, 50 mM Tris (pH 8) and 20% PEG 400. Following centrifugation at 14 000 rpm for 1 min, the supernatant was carefully removed, and the crystals were solubilized in 60 µl of a solution containing 20 mM MES-Tris (pH 7), 20 mM sodium ascorbate and 0.05% αDM at a chlorophyll concentration of 6 mg/ml. A concentrated pea plastocyanin was added into the PSI solution to give final concentration of PSI 2.8 mg Chl/ml and 5 mg/ml plastocyanin. The resulting solution of PSI–Pc (3 µl) was applied on glow-discharged holey carbon grids (Cu Quantifoil R1.2/1.3), before using a Vitrobot FEI (3 s blot at 4°C and 100% humidity). The frozen grids were sent to Dr. Alexey Amunts at the SciLifeLab. Images were collected in the Karolinska Institute (KI) facility using a K3-300 kV FEI Titan Krios electron microscope. The images were collected using a 300 kV FEI Titan Krios electron microscope, with an energy filter of 10 eV. A Gatan K3-Summit detector was used in fast acquisition mode at a magnification of ×130 000 (yielding a pixel size of 0.654 Å), with a total dose of 40.8 e $Å^{-2}$. EPU was used to collect a total of 5310 images, which were dose-fractionated into 51 video frames, with defocus values ranging from 0.3 µm to 1.5 µm. The collected micrographs were motion-corrected and dose-weighted using MotionCor2 [17]. The contrast transfer function parameters were estimated using CtfFind 4.1 [18]. A total of 276 815 particles were picked using reference-free picking using the KLT picker [19]. The picked particles were processed for reference-free 2D averaging, initial model building, 3D classification and refinement resulting in 45 376 particles for intermediate model building; All steps were performed using RELION v.3 [20]. The intermediate model was subsequently used for template-based autopicking in RELION, resulting in 359 977 picked particles. This set was used applied to 2D classification resulting in 141 959 particles, then followed by 3D classification resulting in six distinct classes in RELION. From these, four classes were selected, which contained a total of 104 127 particles. These particles were pooled together and processed for 3D homogeneous refinement and postprocessing using RELION. The reported resolution was based on a gold-standard refinement, applying the 0.143 criterion on the FSC between the reconstructed half-maps. Following data processing (see Methods section) the Pc–PSI supercomplex was modeled at 2.74 Å resolution with local resolution ranging from 2.5 to 4.5 (Supplementary Figure S1).

Model building

To generate the Pc–PSI, the cryo-EM structure of the plant Pc–PSI–Fd model PDB 6YEZ was selected. This model was fitted onto the cryo-EM density map using phenix.dock_in_map in the PHENIX suite [21], and manually rebuilt using Coot [22]. Stereochemical refinement was performed using phenix.real_space_refine in the PHENIX suite [21]. The final model was validated using MolProbity [23]. The refinement statistics are provided in Supplementary Table S1. Local resolution was determined using ResMap [24], and the figures were generated using PyMOL [25] and UCSF Chimera [26]. Representative cryo-EM densities are shown in Supplementary Figure S9.

Chlamydomonas reinhardtii strains and media

Wild type and mutant *C. reinhardtii* strains were grown as described [27]. Tris-acetate-phosphate (TAP) medium was used to grow cells for PSI isolation. The growth tests were performed on solidified (1.5% agar) TAP medium for photoheterotrophic and high salt medium (HSM) for photoautotrophic growth.

Biochemical Journal (2021) 478 2371–2384
https://doi.org/10.1042/BCJ20210267

Isolation of *Chlamydomonas reinhardtii* PSI particles

Whole cells were used for Thylakoid membrane isolation according to established procedures [28]. Afterwards, the isolated membranes were diluted to a chlorophyll concentration of 0.8 mg/ml, solubilized and incubated on ice for 20 min in the presence of 0.9% (w/v) dodecyl β-maltoside. The photosynthetic complexes were separated using a linear sucrose density gradient [29]. The photosystem I was collected and concentrated by using ultra-filtration colums with a size exclusion of 100 000 MW.

Heterologous expression and isolation of *Chlamydomonas reinhardtii* plastocyanin

Plastocyanin was heterologously expressed as described using the *E. coli* BL21 strain. The concentration of the isolated Pc was determined spectroscopically as described [30].

Growth tests

The cell growth at different light conditions was determined by spotting 20 μl of cells from log-phase cultures, which were diluted to the same cell-number (1×10^6 cells/ml) onto agar plates. These plates were kept under 400 μE m^{-2} s^{-1} termed as high light, 40 μE m^{-2} s^{-1} as normal light and 5 μE m^{-2} s^{-1} as low light, respectively. The Genebag Anaerobiosis system provided by BioMérieux was used to establish anaerobic growth.

Generation of mutant strains

The point mutations Asp647Arg, Arg648Asp and Asp647Arg/Arg648Asp in the photosystem I subunit PsaA were introduced by site-directed mutagenesis [31]. The transformation success was confirmed by sequencing as well as the expression and the expression level of the altered photosystem I by Western blot analysis.

SDS–PAGE and Western blot analysis

SDS–PAGE (13% T, 3.45% C) was carried out as published [32]. Proteins were transferred onto a nitrocellulose membrane by semidry electro-blotting. The immuno detection was performed using anti-PsaD and anti-PsaF antibodies for PSI detection in a 1 : 1000 dilution as well as anti-D1 and anti-LhcbM6 antibodies of PSII detection in a 1 : 2000 and 1 : 1000 dilution, respectively.

Single flash absorbance spectroscopy

The kinetics of flash-induced absorbance changes at 817 nm were measured as described before [13] using a cuvette containing 200 μl of the sample with an optical path length of 10 mm. The chlorophyll content was determined according to the protocol published by Porra [33].

NADP-photoreduction measurements

The light driven, PSI dependent reduction in $NADP^+$ was performed as described by Finazzi et al. [34]. The sample was illuminated with saturating light supplied by a halogen lamp with a light intensity of ~10^4 μE m^{-2} s^{-1}.

Multiple sequence alignment (WebLogo)

One-hundred and fifty annotated and reviewed sequences from various photosynthetic phyla where used to generate a multiple sequence alignment using MUSCLE [35] (sequences taken from UniProt). The WebLogo [36] was generated taking subsequence representing the PsaA α-helix l' from the previously generated alignment.

Results

High-resolution structure of reduced plastocyanin in complex with photosystem I

The availability of large amounts of *Pisum sativum* PSI crystals have offered a unique opportunity to solve the structure of photosynthetic supercomplexes by the cryo-EM technique [37]. We have utilized these crystals to form a plant Pc–PSI complex simply by adding purified Pc to pure PSI. To ensure the complex formation the concentration of Pc was kept way above the dissociation constant. Plant PSI was solubilized from stored crystals in a solution containing 20 mM MES-Tris (pH 7), 20 mM sodium ascorbate and 0.05% n-dodecyl-α-maltoside

Biochemical Journal (2021) 478 2371–2384
https://doi.org/10.1042/BCJ20210267

(αDM) at a chlorophyll concentration of 6 mg/ml. Concentrated pea Pc was added into the PSI solution to give final concentration of 2.8 mg Chl/ml PSI and 5 mg/ml Pc. The resulting solution of PSI–Pc (3 μl) was applied on glow-discharged holey carbon grids that were vitrified for cryo-EM structural determination (see Methods). Following data processing (see Methods section) the PSI–Pc supercomplex was solved at 2.74 Å resolution with local resolution ranging from 2.5 to 4.5 (Supplementary Figure S1, Supplementary Table S1, PDB 6ZOO). The structure of Pc–PSI complex is shown in Figure 1. The position on PSI of the reduced Pc is virtually identical with its position in the previously reported Pc–PSI–Fd complex ([37]; PDB 6YEZ). However, improved map densities of Pc (Supplementary Figure S2) allowed a closer look not only at the electrostatic but also potential hydrophobic interactions (Figure 1; Supplementary Movie S1; PDB 6ZOO). Figure 1 shows some of the identified surface interactions where previous molecular biology studies revealed deleterious mutations, with PsaA Trp651 and PsaB Trp627 (Trp658 and Trp625 in pea, respectively) at the center of the hydrophobic binding region [38,39]. Mutagenizing PsaB Glu613 and Asp612 (pea Glu611 and Asn612), which are located in the periphery of Pc binding domain, increased the affinity of Pc binding to PSI alongside with slower Pc release [10,38]. PsaF lysines were observed in close proximity to Pc negatively charged amino acids as reported in [37], with the addition of PsaA Arg117 identified 5.7 Å away from Pc Asp61. Substitution of these lysines disrupted Pc binding, release, and electron transfer to P700 [40]. On the Pc hydrophobic surface, mutating Pro36 — which faces the two tryptophans [41] — as well as Gly10, Leu12, Tyr83 and Ala90 [8,42,43] showed a decreased efficiency in Pc binding and activity. The hydrophobic Pc region involved in PSI–Pc association was suggested to serve a similar role in Pc binding to cytochrome f [44,45].

Photosystem I-plastocyanin binding creates a solvent inaccessible region around plastocyanin's copper while PsaF facilitates plastocyanin release from photosystem I

While structural information readily reveals electrostatic interactions, hydrophobic interactions are much more difficult to decipher [37]. One of the hallmarks of such interaction are the close contacts of the hydrophobic surfaces leaving no space for water molecules. Analysis of the solvent-accessible surface area (SASA) of the Pc binding domain formed by PsaA–PsaB and Pc surface using GetArea with default parameters [46,47] demonstrates that more than 50% of the binding regions become inaccessible to water molecules once the PSI–Pc complex forms, fitting a tightly packed hydrophobic binding (Figure 1B–E, Table 1). These regions are composed of four domains in Pc and five domains in PsaA and PsaB are presented in Figure 1, and several of these amino acids were previously identified as necessary for the transient binding of Pc [8,9,34,37,38,39]. These binding domains display a combination of electrostatic, polar, and hydrophobic interactions with varying magnitudes. Pc domains span from Asp8–Leu12 (domain I), Ala33–Pro36 (domain II), Glu60–Leu62, Asn64–Glu68 (domain III) and Pro86–Gly91 (domain IV). PsaA and PsaB association domains span more intermittently but form five distinct surfaces encircling PsaA Trp658 and PsaB Trp625. The first PsaA surface is formed by Thr635, Ile637–Gly639 and Asn641, the second by Asp655, Trp658, Ala659, Ser662, Gln663, Gln666, Gly669, Ser670 and Leu672 and the third by Arg753, Ala756 and Val757. PsaB first domain consists of Gln603, Asn605 and Gln608, and the second by Arg621, Asp622, Trp625–Asn627, Ser629, Gln630, Asn633, Asn636, Phe638, Asn641, Leu643 and Lys732.

As part of our efforts to describe Pc association and dissociation mechanism, we used in-silico modeling of oxidized Pc from *Populus nigra* ([48]; PDB 4DP9) as our reference. Sequence comparison of Pc from *P. nigra* and pea using BLAST [49] shows a 79% identity (Supplementary Figure S3). The sequence was changed according to pea Pc and then superpositioned on the reduced Pc in 6ZOO. Conformation changes which appeared significant were identified in both Pc acidic patches Asp42–Glu45 and Glu59–Glu60 (Figure 2). The short helix formed by Asp42–Glu45 in oxidized Pc brings Glu43 and Asp44 closer to PsaF Lys93, Lys96 and Lys100, and Glu60 drifts closer to PsaF Lys101 (Figure 2, Supplementary Movie S2). Next, we superimposed the two conformations based on the unchanged PSI interaction region (Asp61–Asn64). In this superposition, the negative patches mentioned before were closer to PsaF Lysines, and tilted relative to the hydrophobic binding region. With this, Pro86–Gly91 moved by 1–4 Å compared with the 6ZOO conformation, leaving ample room for water molecules to accommodate the space between Pc and PSI and drive Pc dissociation from PsaA–PsaB towards PsaF. Inspection of the in-silico model SASA shows that the oxidized Pc surface solvent accessibility increased by 5% compared with the reduced Pc, mostly in the hydrophobic binding patches (Supplementary Table S2).

Biochemical Journal (2021) **478** 2371–2384
https://doi.org/10.1042/BCJ20210267

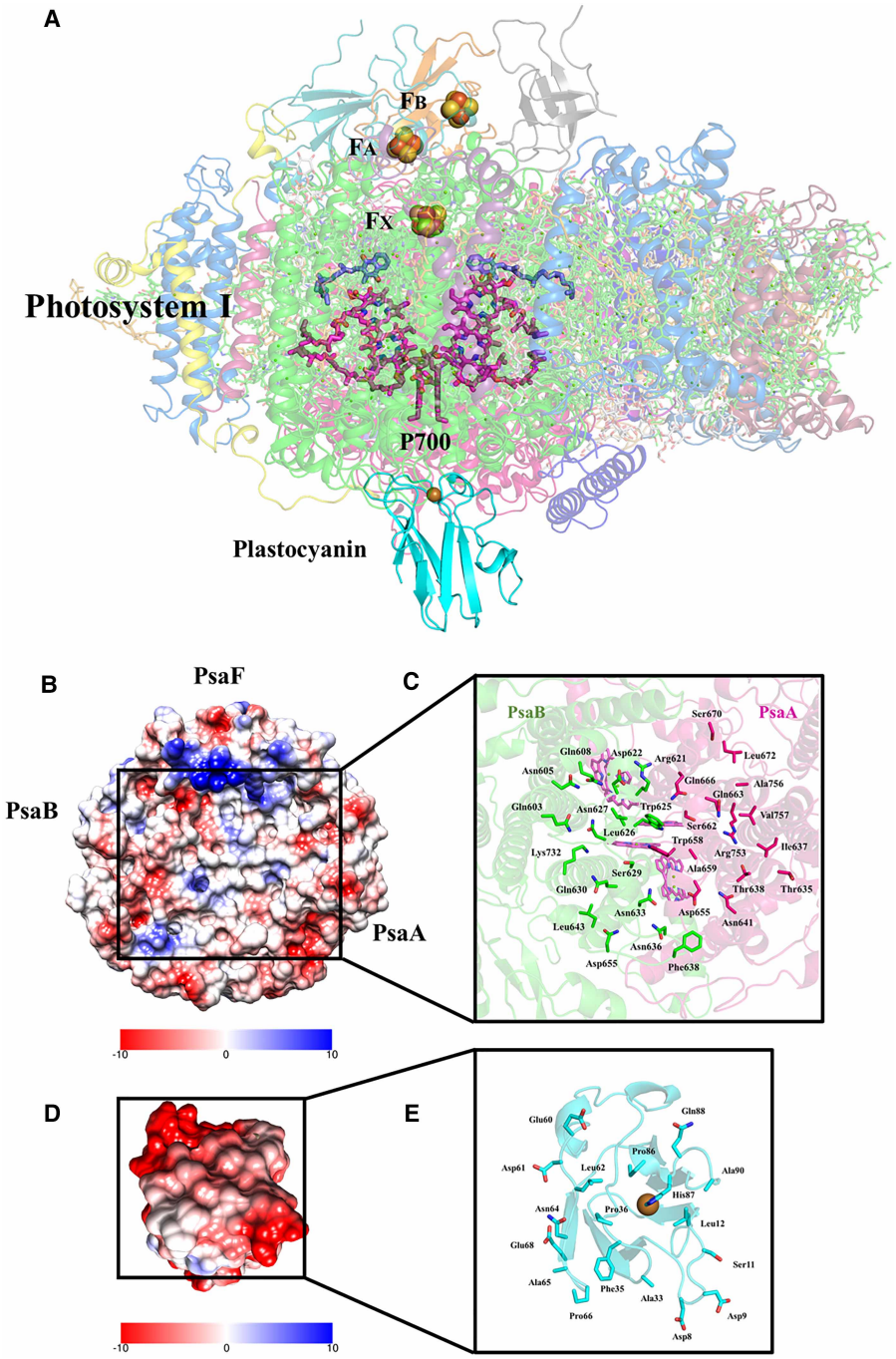

Figure 1. Structure of pea Photosystem I in-complex with reduced pea Pc and analysis of the solvent inaccessible region formed by their bound interfaces.

(**A**) Side view of PSI–Pc complex. (**B**) Electrostatic potential analysis of the Pc binding surface formed by PsaA–PsaB. (**C**) Zoom-in on the PsaA–PsaB amino acids forming the hydrophobic Pc binding surface. (**D**) Electrostatic potential analysis of the Pc region that binds PSI. (**E**) Zoom-in of the Pc amino acids that make up the water inaccessible surface across PsaA–PsaB upon PSI–Pc complex formation.

Biochemical Journal (2021) **478** 2371–2384
https://doi.org/10.1042/BCJ20210267

Table 1. Solvent-accessible surface area (SASA) analysis of Pc, PsaA and PsaB showing a hydrophobic binding area formation during PSI–Pc association

Part 1 of 2

PsaA-PsaB standalone total SASA (Å2)	PsaA-PsaB bound to Pc total SASA (Å2)	Pc total SASA (Å2)	Pc bound to PsaA-PsaB total SASA (Å2)
69660	68854	5226	4343

Residue	Chain	Number	PSI-Pc complex		PSI-Pc unbound		Change%
			Total SASA (Å2)	Ratio%	Total SASA (Å2)	Ratio%	
ASP	Pc	8	94	78	127	97	-18
ASP		9	68	59	140	92	-33
GLY		10	0	0	37	43	-43
SER		11	37	46	63	65	-19
LEU		12	11	4	48	29	-25
ALA		33	19	28	32	48	-20
GLY		34	10	11	38	44	-33
PHE		35	32	17	69	30	-13
PRO		36	5	4	75	71	-67
GLU		60	60	38	156	95	-57
ASP		61	96	81	114	96	-15
LEU		62	24	6	46	21	-15
ASN		64	25	19	91	77	-57
ALA		65	4	2	49	60	-58
PRO		66	43	40	96	90	-51
GLY		67	52	60	54	61	-1
GLU		68	33	20	56	36	-16
PRO		86	14	2	73	31	-29
HIS		87	0	0	32	19	-19
GLN		88	85	55	89	57	-2
GLY		89	12	14	79	91	-77
ALA		90	20	4	63	44	-40
GLY		91	54	62	55	63	-1
			800		1683		
THR	PsaA	635	64	53	90	78	-25
ILE		637	15	6	43	7	-2
THR		638	9	9	23	16	-7
GLY		639	34	39	69	79	-40
ASN		641	18	12	40	31	-19
ASP		655	23	16	29	21	-5
TRP		658	19	6	66	27	-21
ALA		659	10	15	40	52	-36
SER		662	2	3	25	32	-29
GLN		663	10	4	44	28	-24
GLN		666	54	32	80	48	-16
GLY		669	43	49	43	49	0
SER		670	24	22	53	59	-37
LEU		672	25	17	29	20	-3

Continued

Biochemical Journal (2021) **478** 2371–2384
https://doi.org/10.1042/BCJ20210267

Table 1. Solvent-accessible surface area (SASA) analysis of Pc, PsaA and PsaB showing a hydrophobic binding area formation during PSI–Pc association Part 2 of 2

ARG		753	7	4	19	10	-6
ALA		756	19	8	49	27	-19
VAL		757	30	6	53	23	-18
GLN	PsaB	603	65	23	83	36	-12
ASN		605	42	34	57	47	-13
GLN		608	23	13	47	29	-16
ARG		621	30	15	36	18	-3
ASP		622	20	17	24	21	-4
TRP		625	17	5	50	20	-15
LEU		626	6	3	86	54	-51
ASN		627	10	6	11	6	0
SER		629	4	5	38	49	-44
GLN		630	20	13	74	48	-34
ASN		633	6	5	55	47	-43
ASN		636	17	11	31	23	-12
PHE		638	173	78	196	88	-11
ASN		641	35	29	69	59	-30
LEU		643	16	11	18	12	-2
LYS		732	61	19	75	28	-9
			951		1744		

Total — SASA for each residue in Å^2; Ratio — percentage of the area of residue exposed to the solvent; Change — the difference in SASA for each residue, in complex or unbound. Charged or polar amino acids are colored blue, hydrophobic amino acids colored yellow.

PsaA residues R647 and D648 are required for efficient binding and electron transfer between PSI and Pc

To further assess the role of amino acids close to the hydrophobic core represented by PsaA-Trp658, residues PsaA-Arg647 and Asp648 (Arg654 and Asp655 in pea, respectively) were altered via a site-directed mutagenesis approach using *Chlamydomonas reinhardtii* as a model. Notably, Asp648 (pea Asp655) is found at the beginning of the second PsaA surface. Both amino acids PsaA-Arg647 and Asp648 are found very close to Trp651 (pea Trp658) and are also present right at the PsaA–PsaB border. PsaA-Asp648 faces Pc Phe35 directly, and the salt bridge formed by Arg647 and Asp648 (Supplementary Figure S4) prevents them from drifting towards PsaA Trp658 or PsaB Asn633 (pea annotations), the latter found at the interface of the first Pc domain formed by Asp8–Leu12. The coding sequence for both residues in the *psaA* gene was altered to generate a scenario where both encoded residues are positively charged (PsaA-Asp648Arg), both are negatively charged, (PsaA-Arg647Asp) and where the charge is switched (PsaA-Arg647Asp/Asp648Arg). SDS–PAGE fractionation of isolated thylakoid membranes followed by an immuno-blot analysis using anti-PsaD and anti-PsaF antibodies revealed diminished PSI contents of ∼25–75% as compared with wild type, while the PSII content was stable (Supplementary Figure S5).

The second-order electron transfer rates for the electron transfer between Pc and purified PSI complexes were determined via *in vitro* single turnover flashes for excitation at increasing ionic strength (Figure 3A). All genetically modified photosystems revealed a diminished second-order transfer rate as compared with wild type, independent of the salt concentration, with the strongest impact for PsaA-Asp648Arg (Supplementary Table S3).

These findings were supported by light-induced PSI dependent $NADP^+$ reduction measurements in an independent approach. At low Pc concentrations (1.5 μM) the photoreduction rate was about 2-3 times

Biochemical Journal (2021) 478 2371–2384
https://doi.org/10.1042/BCJ20210267

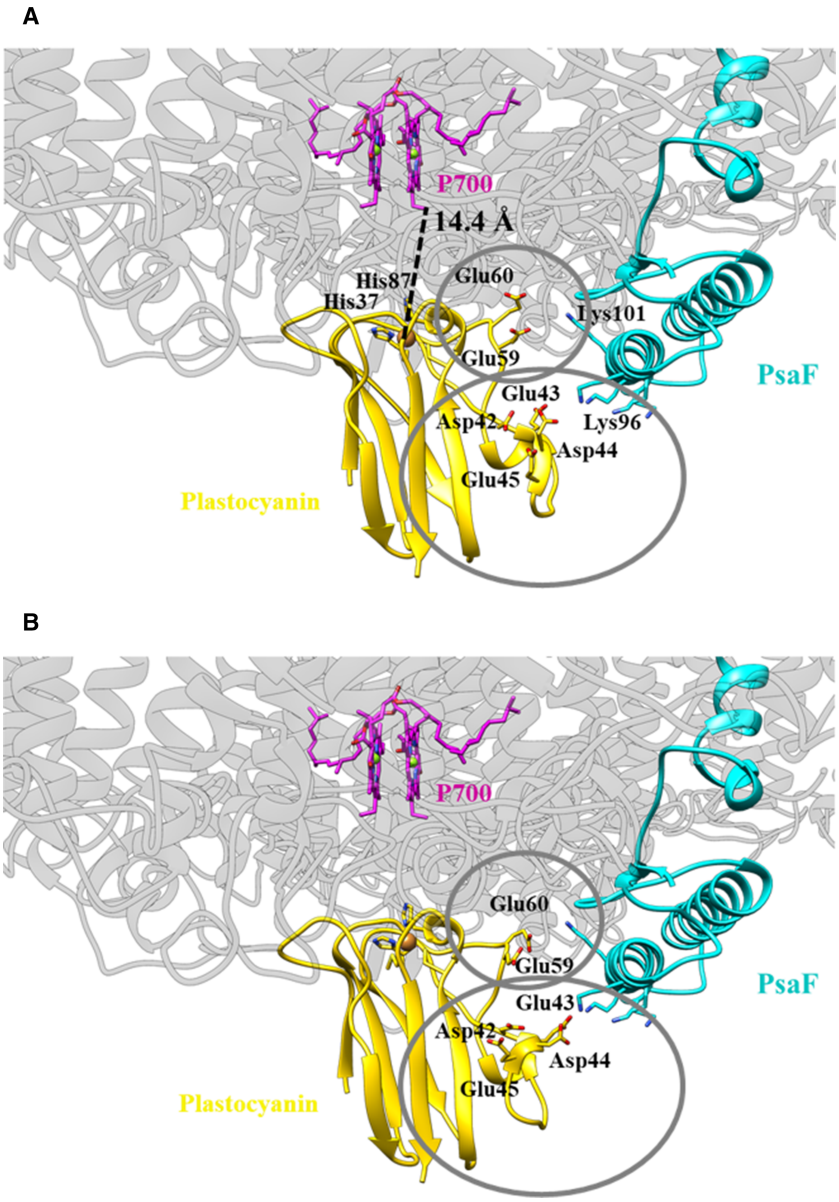

Figure 2. In-silico model of Pc dissociation from PSI.

(**A**) Reduced Pc bound to PSI. Pc acidic patches are marked with a circle. Pc is colored yellow, PSI in light gray, PsaF in cyan and P700 in magenta. Plastocyanin negatively charged amino acids and PsaF Lysines are shown as sticks. (**B**) Oxidized Pc (PDB 4DP9) bound to PSI in-silico. Acidic patches undergo a conformational change, bringing them closer to PsaF positive Lysines.

(PsaA-Arg647Asp, PsaA-Asp648Arg) up to 5 times smaller (PsaA-Arg647Asp/Asp648Arg) for altered PSI was lower as compared with wild type (Figure 3B). Similar effects were observed at high Pc concentrations (80 μM), yet the difference was only about 1.5 times smaller for PsaA-Arg647Asp and PsaA-Arg647Asp/Asp648Arg and 2.5 times smaller for PsaA-Asp648Arg. Both independent approaches indicated an impaired electron transfer from Pc to the altered PSI, independent from the residue combination.

Absorbance transients at 817 nm, induced by fast single turnover flashes, were also recorded at increasing Pc concentrations (Figure 3C). The absorbance transients at high Pc concentrations can be separated into three kinetic components. The fast component A(1) with a constant half-life of 3–4 μs representing the first-order electron transfer reaction within a preformed complex, a second components A(2) with a half-life decreasing at

Biochemical Journal (2021) **478** 2371–2384
https://doi.org/10.1042/BCJ20210267

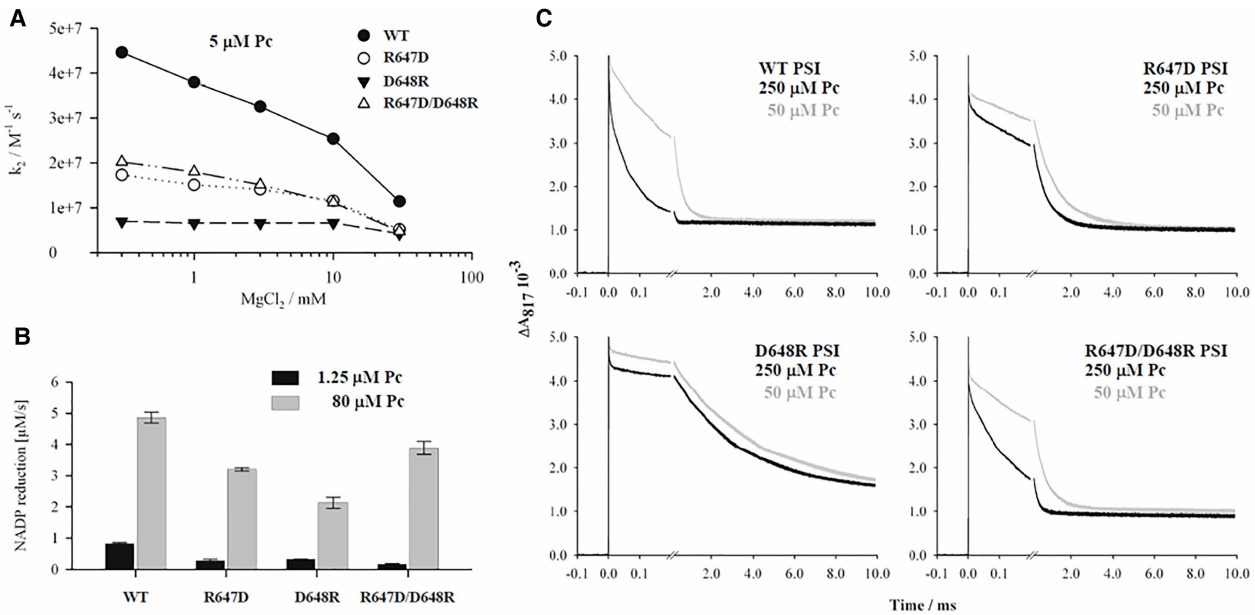

Figure 3. PsaA residues Arg647 and Asp648 are required for an efficient binding of the electron donor Pc.

(**A**) Second-order rate constant of *C. reinhardtii* $P700^+$ reduction by *C. reinhardtii* pc (5 µM) at increasing $MgCl_2$ concentrations. The ionic strength is increased by adding small amounts of concentrated $MgCl_2$ solution. The optimal salt concentration is at 1 mM $MgCl_2$ for wild type and altered PSI, respectively. The second-order electron transfer rate is decreased for all altered photosystems in comparison with wild type. (**B**) Light-driven PSI dependent $NADP^+$ photoreduction measurements for wild type and altered photosystems with pc at low (1.25 mM) and high concentration (80 mM). (**C**) Absorbance transient at 817 nm of the flash-induced photooxidation of wild type and the altered photosystems R647D, D648R and R647D/D648R and their subsequent re-reduction in the presence of 50 and 250 µM pc. The first-order phase shows a half time ∼4 µs, thus the relative amplitude (A1) is smaller in all altered photosystems as compared with wild type (increase of A1/(A1 + A2) from 50 to 250 µM pc, for WT 100%, for R647D 45%, for D648R 17% and for R647D/D648R 30%).

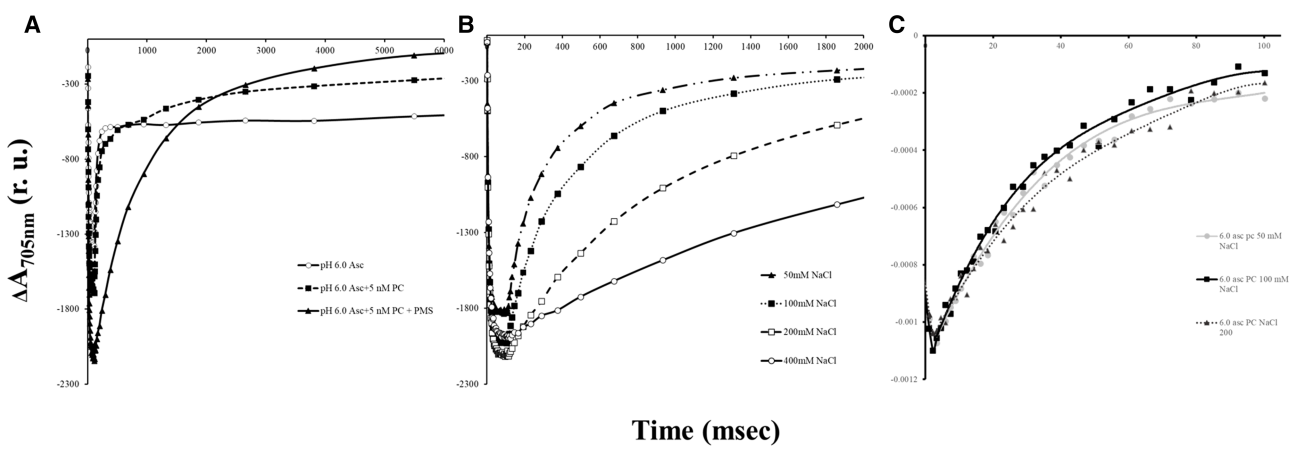

Figure 4. P700 reduction by Pc is dependent on ionic strength and solvent pH.

(**A**) Kinetics of $P700^+$ reduction in plant PSI derived from dissolved crystals in the presence of ascorbate and PMS. The reaction mixture contains: 20 mM MES-Tris (pH = 6.0); 0.05% α-DM and PSI containing 5 µg Chl. Ascorbate — 2 mM; Pc — 5 nM; PMS — 1 µM. Excitation light for 0.1 s. (**B**) Effect of NaCl concentration on the rate of $P700^+$ reduction by pea Pc. The reaction mixture contains: 20 mM MES-Tris (pH = 6.0); 0.05% α-DM and PSI containing 5 µg Chl. All samples contain 10 mM ascorbate, 40 nM Pc. Excitation light duration is 0.1 s. (**C**) NaCl concentration shows no effect on the fast rate of $P700^+$ reduction by Pc. The reaction mixture contains: 20 mM MES-Tris (pH = 6.0); 0.05% α-DM and PSI containing 5 µg Chl. All samples contain 10 mM ascorbate, 40 nM Pc. Excitation achieved by a 10 µs laser flash.

Biochemical Journal (2021) 478 2371–2384
https://doi.org/10.1042/BCJ20210267

higher concentrations indicative of a second-order binding reaction, and a very slow third component A(3) representing PSI complexes that lost their PsaF subunit during the isolation process making up to 25–40% of the total PSI signal [50]. The changes in amplitude of the two faster kinetic components in regard to the donor concentration reflect the binding equilibrium and allows the calculation of the dissociation constant K_D according to Drepper et al. [13]. The K_D value for WT PSI was measured at 88 mM, similar to previous work [40] Determination of the K_D values for all altered photosystems was not possible as the amplitude A(1) did not significantly increase at increasing Pc concentrations, visible in the absorbance transients measured in the presence of 50 and 250 μM Pc (Figure 3C). This reflects a drastically decreased affinity of Pc for the altered photosystems, indicating that changing charges at PsaA residues Arg647 and Asp648 omitted efficient pre-binding of reduced Pc.

Hydrophobic interactions revealed by light-induced P700$^+$ reduction kinetics

Electron transfer measurements were performed using a uniform pea PSI population derived from solubilized diffracting crystals to substantiate that these PSI complexes are very competent in electron transfer. The light-induced P700 oxidation and re-reduction by various electron donors were followed by recording absorption changes at 705 nm using a Joliot-type spectrophotometer (JTS). The signals converted to assume a mM extinction coefficient of 64 at 705 nm [51]. The light-induced absorption change at 705 nm measured by JTS that was calibrated by using plant PSI crystals containing 156 chlorophyll molecules per P700. The standard variation of Chl/P700 ratio from five independent experiments is ±2%, caused mainly due to variation in chlorophyll determination and not the extent of P700 signal.

The data revealed that the reduction in light-induced oxidized P700$^+$ is biphasic with a fast kinetics of ∼100 ms and a slow one of several minutes. The addition of ferredoxin eliminated the fast kinetics. Ascorbate failed to reduce all the population of P700$^+$ and the idle P700 disappeared in the presence of PMS and thus the signal represents the entire P700 population. The presence of PMS eliminated the fast 10 ms back kinetics that was attributed to FB. Only partial elimination of the back reaction was observed in the presence of Pc.

No significant change in OD was observed during illumination from 0.1 to 1 s (Supplementary Figure S6). Similar to ferredoxin and PMS, the presence of methylviologen also eliminated the fast kinetics (Figure 4A). The addition of NaCl significantly decreased the rate of P700$^+$ reduction by Pc (Figures 3A and 4B). Pre-incubation with sufficient Pc amounts should saturate the plastocyanin binding site even under conditions where the electrostatic interactions are eliminated by the presence of high salt concentration. Measurements at a shorter time scale revealed that the A(1) phase, the initial P700$^+$ reduction by pre-bound Pc, is insensitive to the presence of high salt concentration in the reaction mixture (Figure 4C). Under these conditions hydrophobic interactions dominate the Pc binding to PSI, underpinning the importance of such interactions between PSI and Pc.

Discussion

In PSI of oxygenic organisms, the binding site of the reduced electron carriers is mediated by both cytochrome c_6 and Pc. Vascular plants developed specificity for Pc, while cyanobacteria and algae use both as viable electron donors. Three subunits of PSI PsaA, PsaB and PsaF are directly involved in Pc binding [37]. It was reported that the PSI binding site involve both electrostatic and hydrophobic interactions [8,9]. The structure of Pc–PSI supercomplex reveals not only the electrostatic interactions reported before [37] but also hydrophobic interactions (Figure 1B–E, Table 1). It was suggested that the observed kinetics can be explained by a rate-limiting conformational change that occurs in the Pc–PSI complex before the electron transfer takes places [52,53]. We found no significant structural alterations of PSI in response to Pc binding. This is in line with an alternative model, that explains the kinetic properties of the electron transfer between Pc and PSI, where the driving force of the intercomplex electron transfer is decreased to $\Delta G = -55$ meV and tuned for an optimized turnover of PSI [13]. The formation of the intermolecular PSI–Pc complex leads to an exclusion of water molecules as revealed via the structural data (Figure 1). Notably, this is in accordance with a low reorganization energy λ of ∼418 meV, that was determined for the intermolecular electron transfer between Pc and PSI [54], indicating a rather hydrophobic environment at the contact side of both proteins. Thus, electron transfer between Pc and PSI is only coupled to a small reorganization of solvent molecules supporting fast interprotein electron transfer despite relatively low driving force. According to Marcus and Sutin [55], such an exclusion of solvent molecules would result in a decrease in standard entropy of reduction $\Delta S°$ of bound compared with soluble Pc mainly from changes in freedom of the rotation and liberation of the solvent molecules which

surround the reaction partners. Taking advantage of the thermodynamic parameters such as ΔG (free energy change) and λ (the reorganization energy) and an empirical approximation for intraprotein electron transfer [56], an edge-to-edge distance R between Pc and PSI redox centers of 14.5 Å were estimated [54]. This value is very close to the recent structural determination of this distance of 14.4 Å from Cu^+ to P700 CBC_A atom. Therefore, in conclusion, the thermodynamic and structural data are consistent, both supporting the exclusion of solvent molecules from the intermolecular electron transfer complex between PSI and Pc. Interestingly, the exclusion of solvent molecules from the intermolecular complex also has a consequence of the pH-dependent redox midpoint potential of Pc [54].

The importance of the hydrophobic, polar and electrostatic properties formed by the two α-helices *l'* and *j'* for binding of Pc to PSI was further investigated by site-directed mutagenesis of a Arg/Asp residue pair PsaA-Asp648/Arg647. PsaA-Asp648/Arg647 are close to the Trp pair (PsaA-Trp651 and PsaB-Trp627), where indole groups are arranged in a sandwich-like structure above the P700 chlorophyll pair. An alignment of 114 eukaryotic and 36 cyanobacterial PsaA amino-acid sequences revealed a very high sequence similarity, especially for the part of the sequence representing the α-helix *l'* (Supplementary Figure S7). The residues PsaA-Arg647 and PsaA-Asp648 are conserved through all sequences, thus only in *Dinoflagellate* the PsaA-Asp648 is substituted by Asparagine. The single flash absorption measurements revealed diminished second-order rate constants as compared with wild type. The lowest rate was measured for PsaA-Asp648Arg (6.539×10^7 $k_2/M^{-1}\,s^{-1}$). On the other hand, K_D values could not be determined for the electron transfer between Pc and altered PSIs as no or only a minor increase in the A(1) amplitude with increasing Pc concentration was observed. Thus, indicating that the K_D value is substantially increased due to destabilized complex formation between Pc and the altered PSIs. A similar effect was observed for the PsaB-Trp627Phe mutant PSI, where the secondary electron transfer rate was also only slightly diminished, whereas the affinity was strongly impaired. Thus, stable complex formation between PS and Pc is not required for rather productive electron transfer, as revealed by less severe impact on second-order electron transfer constants. However, an exact positioning of electrostatic and polar properties of PsaA-Arg647/Asp648 are required for stable binding of Pc supporting the importance for a precise polar, electrostatic and hydrophobic landscape required for stable complex formation between PSI and Pc. This is also supported by the fact, that high salt concentrations did not impact the formation of the first-order electron transfer complex, while the second-order electron transfer constant was diminished (Supplementary Table S4). This clearly underpins the significance of hydrophobic interactions for stable complex formation between PSI and Pc. The importance of a stable intermolecular electron transfer complex between PSI and Pc is signified by a severe growth phenotype under high light of mutant strains PsaA-D648R, PsaA-R647D and PsaA-R647D/D648R (Supplementary Figure S8). While the polar, electrostatic and hydrophobic landscape is crucial for the tight and stable association between PSI and reduced Pc, it appears to be the weakening of the hydrophobic interaction caused by oxidation of Pc (Supplementary Movie S2), that allows water molecules to accommodate the space between Pc and PSI and that drives Pc dissociation from PSI. This in turn likely explains the six times larger dissociation constant of oxidized Pc as compared with reduced Pc [13], responsible for the 50–60 mV higher midpoint redox potential of Pc bound to PSI.

In summary, the electron transfer between Pc and PSI can be described by the following steps, (i) binding of Pc to PSI facilitated via electrostatic interactions between Pc and PsaF, (ii) stabilization of the reduced Pc–PSI complex due to the hydrophobic as well as polar and electrostatic interface provided by the PsaA and PsaB association domains, (iii) electron transfer from Pc to $P700^+$ within the intermolecular complex, (iv) dissociation of bound oxidized Pc driven via its conformational change, that destabilizes its hydrophobic interaction with PsaA and PsaB interfaces additionally supported through electrostatic pulling towards PsaF.

In conclusion, our data provide mechanistic insights at molecular resolution revealing how the light-driven electron transfer between Pc and PSI was optimized for fast turnover.

Data availability

The atomic co-ordinates have been deposited in the Protein Data Bank, with accession code 6ZOO. The cryo-EM maps have been deposited in the Electron Microscopy Data Bank, with accession codes EMD-11326. All other data are presented in the main text or supplementary materials.

Competing interests

The authors declare that there are no competing interests.

Biochemical Journal (2021) **478** 2371–2384
https://doi.org/10.1042/BCJ20210267

Funding

This work was supported by The Israel Science Foundation (grant no. 569/17), and by German-Israeli Foundation for Scientific Research and Development (GIF) to N.N and M.H., grant no. G-1483-207/2018. M.H. acknowledges support from German Science Foundation (DFG, Hi 739/13-2). N.B-T acknowledges the support of NSF-BSF grant 2019658 and Abraham E. Kazan Chair in Structural Biology, Tel Aviv University.

Author contributions

I.C., M.F., S.K., A.B.-S., D.K., and N.N. performed the research. I.C., F.D., M.H. and N.N. analyzed the data. I.C., M.F., M.H. and N.N. wrote the manuscript. All the authors discussed, commented on and approved the final manuscript.

CRediT Author Contribution

Nathan Nelson: Conceptualization, supervision, funding acquisition, investigation, methodology, writing — original draft, project administration, writing — review and editing. **Ido Caspy**: Data curation, software, formal analysis, validation, investigation, visualization, methodology, writing — original draft, writing — review and editing. **Mariia Fadeeva**: Validation, investigation, methodology. **Sebastian Kuhlgert**: Investigation, visualization, methodology. **Anna Borovikova-Sheinker**: investigation. **Daniel Klaiman**: Investigation. **Gal Masrati**: Investigation. **Friedel Drepper**: Investigation. **Nir Ben-Tal**: Investigation. **Michael Hippler**: Conceptualization, funding acquisition, validation, investigation, methodology, writing — original draft, project administration, writing — review and editing.

Acknowledgements

Dr Yael Levi-Kalisman is gratefully acknowledged and thanked for vitrifying the samples. We thank Dr. Alexey Amunts for data collection in the SciLifeLab Cryo-EM facility, Solna, Sweden. We would like to thank Kevin Redding from the Department of Chemistry and Biochemistry of the Arizona state University for providing the Δ*psaA* strain as well as the plasmid used for site-directed mutagenesis and transformation. Molecular graphics and analyses were performed with UCSF Chimera, developed by the Resource for Biocomputing, Visualization, and Informatics at the University of California, San Francisco, with support from NIH P41-GM103311.

Abbreviations

JTS, Joliot-type spectrophotometer; SASA, solvent-accessible surface area; TAP, tris-acetat-phosphate.

References

1 Nelson, N. and Yocum, C.F. (2006) Structure and function of photosystems I and II. *Annu. Rev. Plant Biol.* **57**, 521–565 https://doi.org/10.1146/annurev.arplant.57.032905.105350
2 Kirchhoff, H. (2014) Structural changes of the thylakoid membrane network induced by high light stress in plant chloroplasts. *Phil. Trans. R. Soc. Lond. B Biol. Sci.* **369**, 20130225 https://doi.org/10.1098/rstb.2013.0225
3 Liu, X., Zhou, Y., Xiao, J. and Bao, F. (2018) Effects of chilling on the structure, function and development of chloroplasts. *Front. Plant Sci.* **9**, 1715 https://doi.org/10.3389/fpls.2018.01715
4 Dalal, V.K. and Tripathy, B.C. (2018) Water-stress induced downsizing of light-harvesting antenna complex protects developing rice seedlings from photo-oxidative damage. *Sci. Rep.* **8**, 5955 https://doi.org/10.1038/s41598-017-14419-4
5 Nelson, N. and Junge, W. (2015) Structure and energy transfer in photosystems of oxygenic photosynthesis. *Annu. Rev. Biochem.* **84**, 659–683 https://doi.org/10.1146/annurev-biochem-092914-041942
6 Höhner, R., Pribil, M., Herbstová, M., Lopez, L.S., Kunz, H.H., Li, M. et al. (2020) Plastocyanin is the long-range electron carrier between photosystem II and photosystem I in plants. *Proc. Natl. Acad. Sci. U.S.A.* **117**, 15354–15362 https://doi.org/10.1073/pnas.2005832117
7 Kirchhoff, H., Schöttler, M.A., Maurer, J. and Weis, E. (2004) Plastocyanin redox kinetics in spinach chloroplasts: evidence for disequilibrium in the high potential chain. *Biochim. Biophys. Acta* **1659**, 63–72 https://doi.org/10.1016/j.bbabio.2004.08.004
8 Haehnel, W., Jansen, T., Gause, K., Klösgen, R.B., Stahl, B., Michl, D. et al. (1994) Electron transfer from plastocyanin to photosystem I. *EMBO J.* **13**, 1028–1038 https://doi.org/10.1002/j.1460-2075.1994.tb06351.x
9 Hippler, M., Reichert, J., Sutter, M., Zak, E., Altschmied, L., Schröer, U. et al. (1996) The plastocyanin binding domain of photosystem I. *EMBO J.* **15**, 6374–6384 https://doi.org/10.1002/j.1460-2075.1996.tb01028.x
10 Kuhlgert, S., Drepper, F., Fufezan, C., Sommer, F. and Hippler, M. (2012) Residues PsaB Asp612 and PsaB Glu613 of photosystem I confer pH-dependent binding of plastocyanin and cytochrome c(6). *Biochemistry* **51**, 7297–7303 https://doi.org/10.1021/bi300898j

11 Schreiber, U. (2017) Redox changes of ferredoxin, P700, and plastocyanin measured simultaneously in intact leaves. *Photosynth. Res.* **134**, 343–360 https://doi.org/10.1007/s11120-017-0394-7
12 Busch, A. and Hippler, M. (2011) The structure and function of eukaryotic photosystem I. *Biochim. Biophys. Acta* **1807**, 864–877 https://doi.org/10.1016/j.bbabio.2010.09.009
13 Drepper, F., Hippler, M., Nitschke, W. and Haehnel, W. (1996) Binding dynamics and electron transfer between plastocyanin and photosystem I. *Biochemistry* **35**, 1282–1295 https://doi.org/10.1021/bi951471e
14 Shimakawa, G. and Miyake, C. (2018) Oxidation of P700 ensures robust photosynthesis. *Front. Plant Sci.* **9**, 1617 https://doi.org/10.3389/fpls.2018.01617
15 Müller, M.G., Niklas, J., Lubitz, W. and Holzwarth, A.R. (2003) Ultrafast transient absorption studies on photosystem I reaction centers from *Chlamydomonas reinhardtii*. 1. A new interpretation of the energy trapping and early electron transfer steps in photosystem I. *Biophys J.* **85**, 3899–3922 https://doi.org/10.1016/S0006-3495(03)74804-8
16 Tian, L., Xu, P., Chukhutsina, V.U., Holzwarth, A.R. and Croce, R. (2017) Zeaxanthin-dependent nonphotochemical quenching does not occur in photosystem I in the higher plant *Arabidopsis thaliana*. *Proc. Natl Acad. Sci. U.S.A.* **114**, 4828–4832 https://doi.org/10.1073/pnas.1621051114
17 Zheng, S.Q., Palovcak, E., Armache, J.P., Verba, K.A., Cheng, Y. and Agard, D.A. (2017) Motioncor2: anisotropic correction of beam-induced motion for improved cryo-electron microscopy. *Nat. Methods* **14**, 331–332 https://doi.org/10.1038/nmeth.4193
18 Rohou, A. and Grigorieff, N. (2015) CTFFIND4: fast and accurate defocus estimation from electron micrographs. *J. Struct. Biol.* **192**, 216–221 https://doi.org/10.1016/j.jsb.2015.08.008
19 Eldar, A., Landa, B. and Shkolnisky, Y. (2020) KLT picker: particle picking using data-driven optimal templates. *J. Struct. Biol.* **210**, 107473 https://doi.org/10.1016/j.jsb.2020.107473
20 Zivanov, J., Nakane, T., Forsberg, B.O., Kimanius, D., Hagen, W.J., Lindahl, E. et al. (2018) New tools for automated high-resolution cryo-EM structure determination in RELION-3. *eLife* **7**, e42166 https://doi.org/10.7554/eLife.42166
21 Liebschner, D., Afonine, P.V., Baker, M.L., Bunkóczi, G., Chen, V.B., Croll, T.I. et al. (2019) Macromolecular structure determination using X-rays, neutrons and electrons: recent developments in Phenix. *Acta Crystallogr. D Struct. Biol.* **75**(Pt 10), 861–877 https://doi.org/10.1107/S2059798319011471
22 Emsley, P., Lohkamp, B., Scott, W.G. and Cowtan, K. (2010) Features and development of Coot. *Acta Crystallogr. D Biol. Crystallogr.* **66**, 486–501 https://doi.org/10.1107/S0907444910007493
23 Chen, V.B., Arendall, III, W.B., Headd, J.J., Keedy, D.A., Immormino, R.M., Kapral, G.J. et al. (2010) Molprobity: all-atom structure validation for macromolecular crystallography. *Acta Crystallogr. D Biol. Crystallogr.* **66**, 12–21 https://doi.org/10.1107/S0907444909042073
24 Kucukelbir, A., Sigworth, F.J. and Tagare, H.D. (2014) Quantifying the local resolution of cryo-EM density maps. *Nat. Methods* **11**, 63–65 https://doi.org/10.1038/nmeth.2727
25 The PyMOL Molecular Graphics System, Version 1.2r3pre, Schrödinger, LLC
26 Pettersen, E.F., Goddard, T.D., Huang, C.C., Couch, G.S., Greenblatt, D.M., Meng, E.C. et al. (2004) UCSF chimera–a visualization system for exploratory research and analysis. *J. Comput. Chem.* **25**, 1605–1612 https://doi.org/10.1002/jcc.20084
27 Harris, E.H. (1989) *The Chlamydomonas Sourcebook*, Academic Press, San Diego, CA
28 Chua, N.H. and Bennoun, P. (1975) Thylakoid membrane polypeptides of *Chlamydomonas reinhardtii*: wild-type and mutant strains deficient in photosystem II reaction center. *Proc. Natl Acad. Sci. U.S.A.* **72**, 2175–2179 https://doi.org/10.1073/pnas.72.6.2175
29 Takahashi, Y., Goldschmidt-Clermont, M., Soen, S.Y., Franzén, L.G. and Rochaix, J.D. (1991) Directed chloroplast transformation in *Chlamydomonas reinhardtii*: insertional inactivation of the psaC gene encoding the iron sulfur protein destabilizes photosystem I. *EMBO J.* **10**, 2033–2040 https://doi.org/10.1002/j.1460-2075.1991.tb07733.x
30 Katoh, S., Shiratori, I. and Takamiya, A. (1962) Purification and some properties of spinach plastocyanin. *J. Biochem.* **51**, 32–40 https://doi.org/10.1093/oxfordjournals.jbchem.a127497
31 Zheng, L., Baumann, U. and Reymond, J.L. (2004) An efficient one-step site-directed and site-saturation mutagenesis protocol. *Nucleic Acids Res.* **32**, e115 https://doi.org/10.1093/nar/gnh110
32 Laemmli, U.K. (1970) Cleavage of structural proteins during the assembly of the head of bacteriophage T4. *Nature* **227**, 680–685 https://doi.org/10.1038/227680a0
33 Porra, R.J., Thompson, W.A. and Kriedemann, P.E. (1989) Determination of accurate extinction coefficients and simultaneous equations for assaying chlorophylls a and b extracted with four different solvents: verification of the concentration of chlorophyll standards by atomic absorption spectroscopy. *Biochim. Biophys. Acta Bioenerg.* **975**, 384–394 https://doi.org/10.1016/S0005-2728(89)80347-0
34 Finazzi, G., Sommer, F. and Hippler, M. (2005) Release of oxidized plastocyanin from photosystem I limits electron transfer between photosystem I and cytochrome b6f complex in vivo. *Proc. Natl Acad. Sci. U.S.A.* **102**, 7031–7036 https://doi.org/10.1073/pnas.0406288102
35 Edgar, R.C. (2004) MUSCLE: multiple sequence alignment with high accuracy and high throughput. *Nucleic Acids Res.* **32**, 1792–1797 https://doi.org/10.1093/nar/gkh340
36 Crooks, G.E., Hon, G., Chandonia, J.M. and Brenner, S.E. (2004) Weblogo: a sequence logo generator. *Genome Res.* **14**, 1188–1190 https://doi.org/10.1101/gr.849004
37 Caspy, I., Borovikova-Sheinker, A., Klaiman, D., Shkolnisky, Y. and Nelson, N. (2020) The structure of a triple complex of plant photosystem I with ferredoxin and plastocyanin. *Nat. Plants* **6**, 1300–1305 https://doi.org/10.1038/s41477-020-00779-9
38 Sommer, F., Drepper, F. and Hippler, M. (2002) The luminal helix I of PsaB is essential for recognition of plastocyanin or cytochrome c6 and fast electron transfer to photosystem I in *Chlamydomonas reinhardtii*. *J. Biol. Chem.* **277**, 6573–6581 https://doi.org/10.1074/jbc.M110633200
39 Sommer, F., Drepper, F., Haehnel, W. and Hippler, M. (2004) The hydrophobic recognition site formed by residues PsaA-Trp651 and PsaB-Trp627 of photosystem I in C*hlamydomonas reinhardtii* confers distinct selectivity for binding of plastocyanin and cytochrome c6. *J. Biol. Chem.* **279**, 20009–20017 https://doi.org/10.1074/jbc.M313986200
40 Hippler, M., Drepper, F., Haehnel, W. and Rochaix, J.D. (1998) The N-terminal domain of PsaF: precise recognition site for binding and fast electron transfer from cytochrome c6 and plastocyanin to photosystem I of *Chlamydomonas reinhardtii*. *Proc. Natl Acad. Sci. U.S.A.* **95**, 7339–7344 https://doi.org/10.1073/pnas.95.13.7339

Biochemical Journal (2021) **478** 2371–2384
https://doi.org/10.1042/BCJ20210267

41 Sigfridsson, K., Young, S. and Hansson, O. (1997) Electron transfer between spinach plastocyanin mutants and photosystem 1. *Eur. J. Biochem.* **245**, 805–812 https://doi.org/10.1111/j.1432-1033.1997.00805.x
42 Sigfridsson, K., Young, S. and Hansson, O. (1996) Structural dynamics in the plastocyanin-photosystem 1 electron-transfer complex as revealed by mutant studies. *Biochemistry* **35**, 1249–1257 https://doi.org/10.1021/bi9520141
43 Jansson, H., Okvist, M., Jacobson, F., Ejdebäck, M., Hansson, O. and Sjölin, L. (2003) The crystal structure of the spinach plastocyanin double mutant G8D/L12E gives insight into its low reactivity towards photosystem 1 and cytochrome f. *Biochim. Biophys. Acta* **1607**, 203–210 https://doi.org/10.1016/j.bbabio.2003.09.011
44 Ubbink, M., Ejdebäck, M., Karlsson, B.G. and Bendall, D.S. (1998) The structure of the complex of plastocyanin and cytochrome f, determined by paramagnetic NMR and restrained rigid-body molecular dynamics. *Structure (London, England: 1993)* **6**, 323–335 https://doi.org/10.1016/s0969-2126(98)00035-5
45 Illerhaus, J., Altschmied, L., Reichert, J., Zak, E., Herrmann, R.G. and Haehnel, W. (2000) Dynamic interaction of plastocyanin with the cytochrome bf complex. *J. Biol. Chem.* **275**, 17590–17595 https://doi.org/10.1074/jbc.275.23.17590
46 Fraczkiewicz, R. and Braun, W. (1998) Exact and efficient analytical calculation of the accessible surface areas and their gradients for macromolecules. *J. Comput. Chem.* **19**, 319–333 https://doi.org/10.1002/(SICI)1096-987X(199802)19:3<319::AID-JCC6>3.0.CO;2-W
47 Fraczkiewicz, R. and Braun, W. (1996). A New Efficient Algorithm for Calculating Solvent Accessible Surface Areas of Macromolecules. Presented at the Third Electronic Computational Chemistry Conference, Northern Illinois University, IL
48 Kachalova, G.S., Shosheva, A.C., Bourenkov, G.P., Donchev, A.A., Dimitrov, M.I. and Bartunik, H.D. (2012) Structural comparison of the poplar plastocyanin isoforms PCa and PCb sheds new light on the role of the copper site geometry in interactions with redox partners in oxygenic photosynthesis. *J. Inorg. Biochem.* **115**, 174–181 https://doi.org/10.1016/j.jinorgbio.2012.07.015
49 Altschul, S.F., Gish, W., Miller, W., Myers, E.W. and Lipman, D.J. (1990) Basic local alignment search tool. *J. Mol. Biol.* **215**, 403–410 https://doi.org/10.1016/S0022-2836(05)80360-2
50 Hippler, M., Drepper, F., Farah, J. and Rochaix, J.D. (1997) Fast electron transfer from cytochrome c6 and plastocyanin to photosystem I of *Chlamydomonas reinhardtii* requires PsaF. *Biochemistry* **36**, 6343–6349 https://doi.org/10.1021/bi970082c
51 Hiyama, T. and Ke, B. (1972) Difference spectra and extinction coefficients of P 700. *Biochim. Biophys. Acta* **267**, 160–171 https://doi.org/10.1016/0005-2728(72)90147-8
52 Bottin, H. and Mathis, P. (1985) Interaction of plastocyanin with the photosystem I reaction center: a kinetic study by flash absorption spectroscopy. *Biochemistry* **24**, 6453–6460 https://doi.org/10.1021/bi00344a022
53 Bottin, H. and Mathis, P. (1987) Turn-over of electron donors in photosystem I: double-flash experiments with pea chloroplasts and photosystem I particles. *Biochim. Biophys. Bioenerg.* **892**, 91–98 https://doi.org/10.1016/0005-2728(87)90251-9
54 Hippler, M., Drepper, F. and Haehnel, W. (1995) The oxidizing site of Photosystem I modulates the electron transfer from plastocyanin to P700+. In *Photosynthesis : from light to biosphere; proceedings of the Xth International Photosynthesis Congress* (Paul Mathis ed.), Kluwer Acad. Publ. Montpellier, France
55 Marcus, R.A. and Sutin, N. (1985) Electron transfers in chemistry and biology. *Biochim. Biophys. Rev. Bioenerg.* **811**, 265–322 https://doi.org/10.1016/0304-4173(85)90014-X
56 Moser, C.C., Keske, J.M., Warncke, K., Farid, R.S. and Dutton, P.L. (1992) Nature of biological electron transfer. *Nature* **355**, 796–802 https://doi.org/10.1038/355796a0